Twist-channel angular pressing: effect of the strain path on grain refinement and mechanical properties of copper

Radim Kocich · Jaroslav Fiala · Ivo Szurman · Adéla Macháčková · Milan Mihola

Abstract Substructural characteristics of Cu (99.97%) were examined after the Twist channel angular pressing (TCAP) process carried out at ambient temperature. Grain refinement efficiency and resulting thermal stability were evaluated after three passes with respect to utilization of various strain paths. Results were obtained using light microscopy and X-ray diffraction methods; Mechanical properties of extruded materials were also tested. Thermal stability was studied after application of three annealing cycles. Based on the findings, *Bc* route is the most efficient strain path with respect to the grain refinement; higher speed of extrusion (10 mm/s) corresponds with suppression of the static recrystallization. Measured strength, obtained after three passes (route *A*), achieved values around 440 MPa homogeneously along the cross section of the extruded material. Homogeneity of deformation was also confirmed by micro-hardness tests. The grain size, determined after three passes, averaged out 1.2 μm. Application of TCAP (three passes) brought markedly homogeneous deformation throughout the processed sample in comparison with classical ECAP process.

R. Kocich (✉)
Department of Material Forming, Faculty of Metallurgy and Materials Engineering, VŠB TU Ostrava, 17.listopadu 15, Poruba, 70833 Ostrava, Czech Republic
e-mail: radim.kocich@vsb.cz

J. Fiala
Department of Material Engineering, Faculty of Metallurgy and Materials Engineering, VŠB TU Ostrava, 17. listopadu 15, Poruba, 70833 Ostrava, Czech Republic

I. Szurman
Department of Non Ferrous Metals-Refining and Recycling, Faculty of Metallurgy and Materials Engineering, VŠB TU Ostrava, 17.listopadu 15, Poruba, 70833 Ostrava, Czech Republic

A. Macháčková
Department of Thermal Engineering, Faculty of Metallurgy and Materials Engineering, VŠB TU Ostrava, 17. listopadu 15, Poruba, 70833 Ostrava, Czech Republic

M. Mihola
Department of Robotics, Faculty of Mechanical Engineering, VŠB TU Ostrava, 17. listopadu 15, Poruba, 70833 Ostrava, Czech Republic

Introduction

In recent years, SPD (severe plastic deformations) methods have proved to be a useful tool in the process of microstructure refinement, which allowed enhancing of the strength properties while preserving good ductility [1–3]. At the same time, as has been shown experimentally, mechanical properties can be improved without significant debilitation of the utility properties of materials manufactured in this manner [4–7].

Many technologies based on SPD methods have emerged recently, such as equal channel angular pressing (ECAP) [8–13], high pressure torsion (HPT) [14], twist extrusion (TE) [15, 16], cyclic extrusion compression (CEC) [17, 18], or C-shape equal channel reciprocating extrusion (CECRE) [19] have been developed. Recent development of ECAP method also gave rise to some new technological operations such as non-equal channel angular pressing (NECAP) [20] and twist channel angular pressing (TCAP) [21].

Plastic strain in ECAP process is accomplished by utilization of the known paths *A* (no rotation between passes), *Ba* (±90° rotation between passes), *Bc* (+90° rotation between passes), and *C* (180° rotations between passes).

The effects of utilized strain paths on microstructure and grain refinement were evaluated using various materials; however, most of the experiments were carried out using Al or Al-based alloys [22–29]. It is also well known that various shear systems can be activated depending on the used strain path during ECAP [9, 10, 29]. Even the effectiveness of the creation of the equiaxed microstructure can be evaluated according to the way of extrusion. The order of the strain path effectiveness on grain refinement is different. According to Refs. [30–32], the *Bc* path is the most effective path in the case of application of a die with a 90° angle. The second most effective path is *C* and the *A* path is the least effective. Information from Segal [33] has brought certain justification of this finding. He states that the creation of shear bands along the shear surfaces is a probable reason for this sequence. Repeating of the process produces transformation of the shear bands created during the previous passes.

Gholinia et al. [22] came to different conclusions during his study of the effectiveness of the strain paths. He carried out his experiment on Al alloys with application of a die with a 120° angle. According to his conclusions, the most effective method of the submicrometer grain structure creation by severe plastic strain is the *A* path. The strain is accumulated in a more effective way thanks to the constant strain path. The *C* and *Bc* paths are procedures with an excessive (redundant) strain. As a redundant strain is called process where the shear strain of one pass (*n*) is reversed by the strain at each 2*n* passes, and each 4*n* passes. This factor makes them less effective during the HAGBs (high angle grain boundaries) creation in comparison with the *A* path.

Every even passage decreases (removes) the imposed shear strain during the application of the *C* path. It prevents the creation of a larger amount of new grains with HAGBs. The sample is also deformed on two alternating planes on the *Bc* path, but the total strain becomes redundant after every fourth passage. Nevertheless, one of the reasons for these conclusion (route *A* is the most effective route) can be the fact that during ECAP with 120° die is not imposed enough strain to prevent structure reversion process.

A redundant strain according to Embury et al. [34] is another factor that influences the course of the restoration processes, especially recrystallization. A smaller amount of stored energy and density of highly rotated regions are the main reasons. These regions can act as nuclei of the new grains. Other authors Refs. [35, 36] state that the combination of the shear bands plays a primary role during the refinement, while the size of the accumulated strain is a secondary factor.

The efforts of the authors are focused on more effective grain refinement and particle redistribution on the basis of the described information. This objective is fulfilled, for example, by modification of the existing strain paths [37]. The real solution is based on the proposal of a new deformation route $B_{C\text{-}UD2}$ (ECAP route) executed on the basis of the transformation matrix analysis. The route $B_{C\text{-}UD2}$ follows route *Bc* but the sample is put upside down once every two passes. Development of these efforts by the more effective ways of refinement of fine homogeneous structure during ECAP was also an objective of this article. The amount of imposed strain per one passage is one of the limits of this method. Inhomogeneity of the strain through

Fig. 1 Principle of TCAP process in comparison with ECAP, with shearing characteristics for deformation routes *A*, *Ba*, *Bc*, and *C*; *cw* clockwise rotation, *ccw* counterclockwise rotation; *red line* in the plane denotes its position after individual pass (up to four passes)
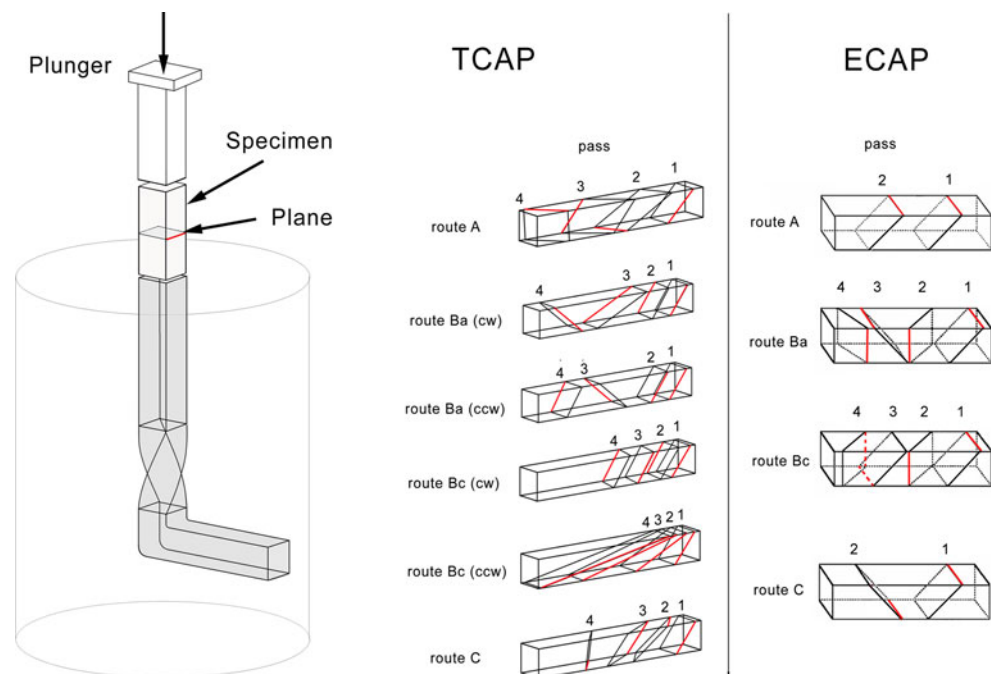
the cross section of the extruded material is another factor. It results from the essence of placement and shape of the intersection plane between channels (different velocities of upper and lower part of the processed sample). This inhomogeneity causes heterogeneity of the grain size. The described reasons have led us to the proposal of the TCAP technology [21].

The main objective of the experiment was mapping of the influence of the strain paths on the development of the deformed structures during the TCAP process. Among other things, the "known" deformation routes as well as their mutations are described in this article. TCAP effectiveness during the grain refinement was also monitored. This was related to the mapping of the restoration processes. Information about the material behavior from the standpoint of final properties of the processed material was also part of the experiment.

Experimental material and procedures

The TCAP process schematic diagram is shown in Fig. 1. The experiment itself consisted of three passages. The deformation routes known from the ECAP technology were used, i.e., A (no rotation), Ba ($\pm 90°$ rotation), Bc ($+90°$ rotation), and C (180° rotation). It is obvious from the principle of the process itself (Fig. 1) that thanks to the die design the torsion precedes the bending itself. If the strain paths will be defined in the same way as in the standard ECAP [30], the same shear systems will not be activated during them. In the case of ECAP process (e.g., route A—the strain is imposed on same slip system with subsequent passes) in comparison with TCAP process where due to twist the sample will be rotated in specific direction. That is why the imposed strain will not be accumulated on the same shear system as in the ECAP process. The shear strain is applied first of all on the processed material during the TCAP in the part of the channel where the torsion is situated. This causes a substantial shear strain especially in the periphery areas of the extruded material. The sample is exposed to shearing subsequently. Further strain is imposed into the sample here that is placed mainly in the central areas (as has been proved by a numerous experiments [38–40]). Figure 1 shows the change of orientation and possibly behavior of an "imaginary" plane in the sample during the TCAP process. It is marked schematically for all implemented strain paths.

Cu with commercial purity of 99.97% was used for the experiment. The exact composition of the experimental material is shown in Table 1. TCAP was carried out at room temperature (RT). Cu after the thermal treatment in the mode 600 °C/30 min was used as the initial material. Thermal processing was carried out with the objective of

Table 1 Chemical composition of copper (wt%)

Element	Zn	Sn	Fe	Ni	Si	Cu
Content	0.0030	0.0058	0.0031	0.0074	0.0023	Bal.

obtaining a fully recrystallized state, and possibly to eliminate a previous history of forming. The samples had a rectangular cross section, length 80 mm, and cross section dimensions 8 × 8 mm. The extrusion was executed at a press crossbar rate of 5 mm/s and the RT. The extrusion on the Bc route at the rate of 10 mm/s was also executed for determination of the influence of a higher strain rate.

Three modes of thermal processing were applied on TCAP in the samples later. You can find detailed information on the annealing processes in "Thermal treatment of samples after TCAP".

The microstructure of the processed copper was investigated by optical microscopy (OM) using an Olympus GX51 optical microscope with computerized imaging system and evaluation software. The mean grain size was calculated using the "analySIS work" software package by Olympus Soft Imaging Solutions GmbH

X-ray diffraction (XRD) was used for determination of the presence of restoration processes. The MICRONA I machine with semi-focusing Bragg–Brentano arrangement was used. Final XRD patterns were made by photoregistration of all the processed samples. Azimuthal profiles of the diffraction line planes (1 1 1) and (2 0 0) were also carried out by means of counting registration.

Mechanical properties of the processed copper were evaluated by tensile tests. All tensile tests were done on an Instron 3382 machine at RT. In addition, measurements of Vickers micro-hardness (HV100) of the Cu were carried out with a micro-hardness tester of type FM ARS 900 (Future Tech) equipped with a diamond Vickers indenter (100 N, indentation time 15 s).

Results and discussion

Cu mechanical properties after TCAP

Specimens for the tensile tests were taken from surface areas (PR) as well as central areas (CR) of extruded material (Fig. 2). The homogeneity of mechanical properties at the specimen cross section was investigated in this way. The testing was carried out on all processed specimens. Figure 2 shows obtained courses of true stress–true strain after three passes. It is obvious that the differences among the achieved strength values between CR and PR are very small. Table 2 summarizes the achieved mechanical properties after the tensile test, if all strain paths are used.
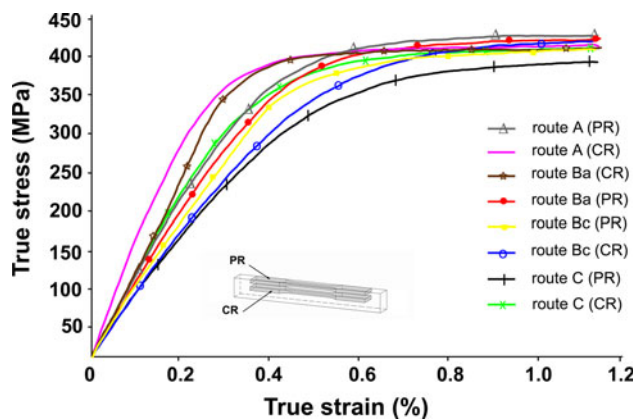
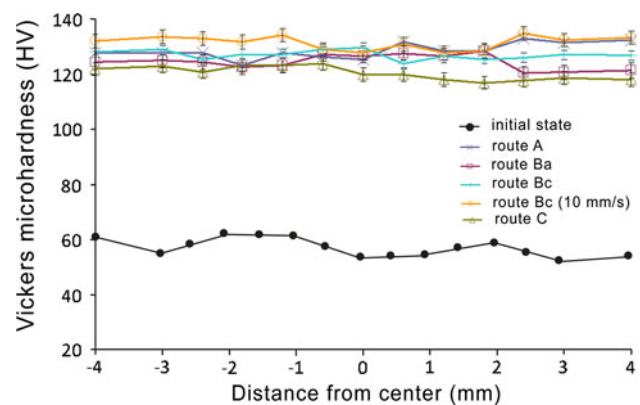**Fig. 2** True stress–true strain curves after TCAP (three passes) for chosen routes

Fig. 3 Micro-hardness distribution over cross section of processed samples

Table 2 Mechanical properties of TCAP-processed Cu samples

Sample	YS (MPa)	UTS (MPa)	δ (%)	E (GPa)	(YS $\times$ δ/100)
0 (initial state)	70	207	47.7	–	33
I (route *A*)	408	438	12.5	115	51
II (route *Ba*)	404	439	12.5	110	50
III (route *Bc*)	392	409	8.3	118	33
IIIv (route *Bc*)[a]	395	420	8.3	114	33
IV (route *C*)	358	379	16.7	106	60

[a] Higher velocity of extrusion (10 mm/s)

It is obvious from the results shown in Table 2 that the yield strength was growing in the following sequence: $C < Bc < Ba < A$. The sequence is reversed in comparison with the sequence described by Dobatkin [41]. However, we have to take into account the fact that the published results are related to oxygen-free copper after the classical ECAP process. The sequence is different if we take into account the sequence determined by the formula YS $\times$ (δ/100) (meaning quality number) where YS is yield strength and δ is ductility. The quality number changes the path sequence so it will approach the sequence determined by Dobatkin $C \geq A \geq (Ba, Bc)$.

As has been described above, all deformation routes are modified by the sample rotation. It means that different shear systems are activated in comparison with ECAP. Aside from this factor there is also the factor of the sample rotation direction before the extrusion itself. A similar situation can also be found with the TE process [42] or HPT [43]. This factor will play a substantial role especially on the strain paths Ba and Bc. The activated shear system will depend on the direction of rotation (cw-clockwise or ccw-counterclockwise) during these procedures. This means that the TCAP process enables the creation of new mutation of the existing strain paths: Bc (cw), Bc (ccw), Ba

(cw), Ba (ccw) (Fig. 1). All of the described facts will influence the development of deformation structures. It is necessary to emphasize that the procedure will be different in comparison with the ECAP standard technology. This enables clarification of differences in the obtained values in comparison with Dobatkin. It is expected generally that the property changes are caused by the overall grain refinement [44, 45]. As has been explained already, each path during the ECAP is characterized by given effectiveness during the grain fining. It is also reflected in the changes of actual properties and it is also valid in the case of TCAP technology.

Micro-hardness after TCAP

The influence of the strain paths on the achieved micro-hardness was evaluated after the extrusion. HV 100 micro-hardness measurement was carried out on the whole width of the sample cross sections. Attention was paid to the fact that the individual indentations must be placed sufficiently far from each other. In total, about 36 indentations were made on each sample. Figure 3 shows distribution of the micro-hardness values on the cross sections (at mid-length) of the extruded samples.

The highest micro-hardness values were determined on the samples processed by the Bc route (10 mm/s) and also on the sample extruded by the route A at lower speed (5 mm/s). Conversely, the C route is the "least" strain strengthening path. The values of micro-hardness achieved after all applied paths have increased at least two times. These conclusions correspond very well with the tensile test results. All extruded materials show a very high homogeneity of micro-hardness. The homogeneity of the micro-hardness values is more or less the same regardless of the used strain path. This conclusion is also valid for the extrusion at a higher strain rate. That conclusion is supported by recently published conclusions on homogeneity

of applied strain distribution in the TCAP process [21]. It should be emphasized that the equivalent strain after the single passage reached at minimum values ~2.1 across the most of the sample.

Microstructure after TCAP

The microstructure of a cross section of the initial Cu sample before extrusion (after annealing in the mode 600 °C/30 min) is shown in Fig. 4a. The sequence of the Fig. 4b–e maps the microstructures after the extrusion (after the third passage) at the individual strain paths.

The bigger grains are relatively evenly distributed after the route A (Fig. 4b). The grains smaller than 10 μm are placed among them. Neither the smaller nor the bigger grains show a priority orientation (elongation) in any direction. It is related to the element behavior described in Fig. 1 with a very high probability. The sample deformed by route Ba has shown similar behavior, but unlike in the previous case there was no creation of "islands" of bigger grains as in the case of the A route. However, the presence of a lesser amount of the bigger grains has been confirmed. There is a different situation in the case of utilization of the Bc route (Fig. 4c). We can see the presence of almost all grains smaller than 5 μm in one direction. Distinct differences are visible after pressing by Bc route (10 mm/s) (Fig. 4d) in comparison with the same path at a lower speed (5 mm/s). A preferential arrangement of some grains in the given direction can also be observed. The route C has brought the biggest heterogeneities of the grain sizes (Fig. 4e).

It is evident that the extrusion has brought about considerable homogenization of the grain size. In spite of this the structures show a relatively bimodal grain distribution especially after certain paths (for example C). First of all the fine grains in some areas are arranged in the form of bands. Similar results were also found by Zhang and Shim [46] after ECAP on Cu. He detected localized strain bands containing grains that are smaller than the size of the grains located outside of these bands. The sizes of the grains inside these bands decrease with the strain rate increase. In certain cases, a rotational dynamic recrystallization can take place at higher strain rates in the vicinity of these bands according to Refs. [47, 48]. Very fine grains (with the size of several nanometers) are created as a consequence of the recrystallization.

We make assumptions from OM about the differences among the individual strain paths. XRD was used for the determination of more comprehensible differences.

XRD of Cu samples after TCAP

XRD was used mainly with the aim of obtaining information on the restoring processes of the processed Cu as well as for further characterization of the structure. Distinction of some differences arising from OM was another established aim. Among other things the testing was focused on the distinction of dynamic or static processes. XRD was established by investigation of appearance of azimuthal profile of diffraction lines of the mosaic blocks (Coherent Scattering Regions) in structure of Cu.

Initial state (sample 0)

The sample has a rough mosaic structure after applied annealing (before TCAP). The blocks are usually much bigger than 10 μm and they have uneven edges (Fig. 5a). All of these findings were caused by previous thermal treatment.

Route A (sample I), route Ba (sample II)

The size of the mosaic blocks of the samples I and II has decreased substantially after three passages. It was also valid for their disorientation in comparison with the initial state. The samples showed all mosaic blocks smaller than 10 μm (Fig. 5b).

Route Bc (sample III)

Substantial decreasing of the mosaic block size as well as their disorientation was also determined on the sample III. The mosaic blocks were usually smaller than 10 μm, but some new ones also appeared. These blocks are perfect, and they are markedly separated from the fine-grained matrix. The new mosaic blocks are bigger than 10 μm. The amount of these new big blocks is relatively low. There is no doubt about the course of the primary recrystallization thanks to their presence. The recrystallization occurred only after the executed strain. This means that the dynamic recrystallization did not come about during the strain (boundary between the new grains and the matrix would be uneven). It implies that a static recrystallization took place as a consequence of imposed strain. In spite of the fact that the whole process took place at RT, there was a temperature increase (up to 53 °C) [21] at the place of shearing as a consequence of the sample friction. The accumulated energy of the plastic strain probably contributed to the activation of nucleation and growth of the new "dislocationless" mosaic blocks. The energy difference between the deformed and recrystallized metal was the driving force of the process.

Route Bc (sample IIIv)

The analysis of the sample extruded at a higher speed (10 mm/s) by the Bc route confirmed a dramatic decrease

Fig. 4 Microstructure of copper and corresponding grain size distribution. **a** initial state; **b** after TCAP (route *A*, 5 mm/s); **c** after TCAP (route *Bc*, 5 mm/s); **d** after TCAP (route *Bc*, 10 mm/s); and **e** after TCAP (route *C*, 5 mm/s)
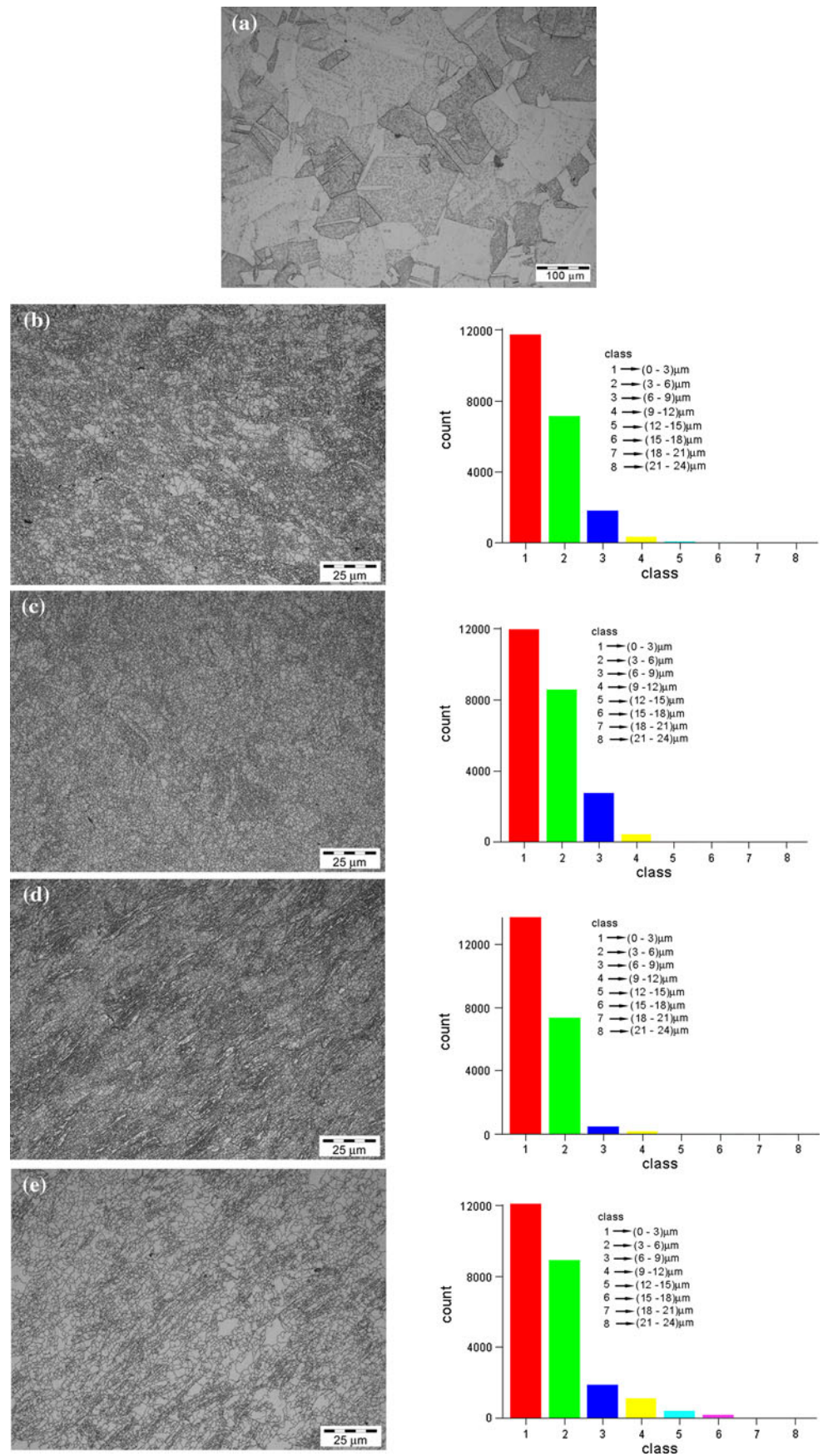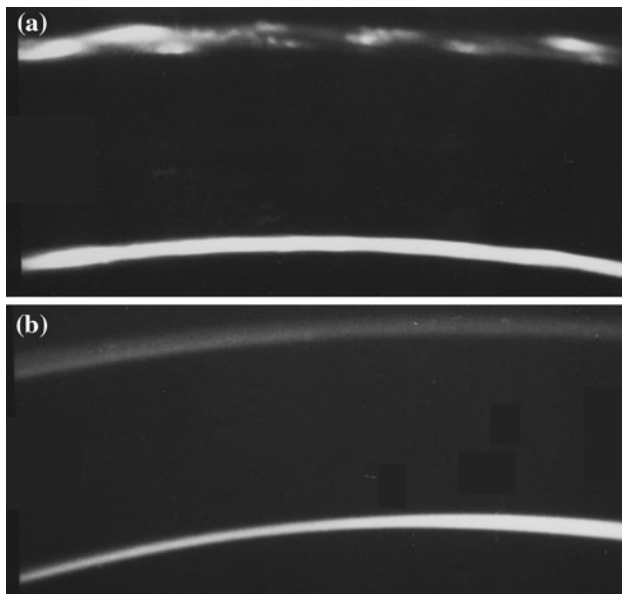
Fig. 5 X-ray diffraction lines of the planes (1 1 1) and (2 0 0). **a** Initial state (before TCAP) and **b** after TCAP (route *A*, 5 mm/s)

of the mosaic block sizes as well as their disorientation. All mosaic blocks are smaller than 10 μm. The static recrystallization of the extruded sample did not take place in this case. It is a different course in comparison with the sample extruded by the same route, but at a lower speed (recrystallization passed off). The higher extrusion rate or the higher strain rate is a probable reason. It supports the finding that the nucleation of the new mosaic blocks (i.e., the restoration process) takes place during strain in a dynamic way. Therefore, the higher strain rate does not have enough time for its course.

Route C (sample IV)

The size of the mosaic blocks and their disorientation in comparison with the initial state decreased dramatically after three passes. The mosaic blocks are usually smaller than 10 μm. A portion of the blocks in the structure are bigger than 10 μm. They are perfect and they are markedly separated from the fine-grained matrix (without recrystallization). The primary recrystallization took place during the route *C*. The process did not pass during the extrusion, but only after it. It means that even the sample deformed by the *C* route recrystallized in a static way.

The material structure character at the initial state as well as after the extrusion is in accordance with the mechanical properties (Table 2). They are in accordance even in such details as strength of the sample IIIv, which is markedly higher than in the case of the sample III. The factor of the lower strain rate enabled the course of recrystallization and strengthening in the sample III. These

processes did not take place in the sample IIIv. Similar results were published by Kadri and Hartwig [49] who demonstrated that the increased plastic strain of copper by multi-pass ECAP decreases recrystallization temperature during the heat treatment.

Thermal treatment of samples after TCAP

The deformed samples were placed into the furnace for the determination of thermal stability after TCAP and they were heated at a constant rate up to the requested temperature with a subsequent dwell at this temperature. The thermal treatment was executed in three selected modes. Mode (R1) → 280 °C/15 min, mode (R2) → 400 °C/ 15 min, and mode (R3) → 500 °C/15 min. All thermal treatment modes were carried out in the protective atmosphere (Ar_2).

Micro-hardness after TCAP and thermal treatment

The micro-hardness was evaluated by the same method as in the case of deformed samples after the executed annealing in the modes R1–R3. The obtained values after R1 are slightly higher in comparison to the state before TCAP with respect to the temperature of the annealing (Fig. 6a, b, and c). The situation during comparison of the individual strain paths is completely different. While the material shows the highest micro-hardness values in the case of the *Bc* route (10 mm/s) after R1 mode, the hardness drops to the level of other samples after the R2 mode. So the higher extrusion rate also meant a higher thermal stability (up to the temperature of 280 °C) in comparison with the lower extrusion rate. Nevertheless, the influence of the higher rate is removed at the higher temperatures (R2, R3) and the values of micro-hardness are very similar. The determined difference is probably related to the course of the static restoration processes. The higher extrusion rate caused a limitation of the static recrystallization course.

On the contrary, the most stable values of micro-hardness at the higher temperatures can be found in Cu after the *C* route.

Microstructure after TCAP and thermal treatment

R1 mode The microstructures after the paths *A* and *Ba* and subsequent R1 annealing are very similar (Fig. 7a). Homogenizing of the grain sizes took place in both samples. However, the bimodal distribution can be found only locally in the structure after the annealing. It should be said that the grain size is more uniform. There is a different situation after deformation by the route *Bc* (Fig. 7b) and subsequent annealing. Even here the homogenizing of the grains size took place in comparison with the state before
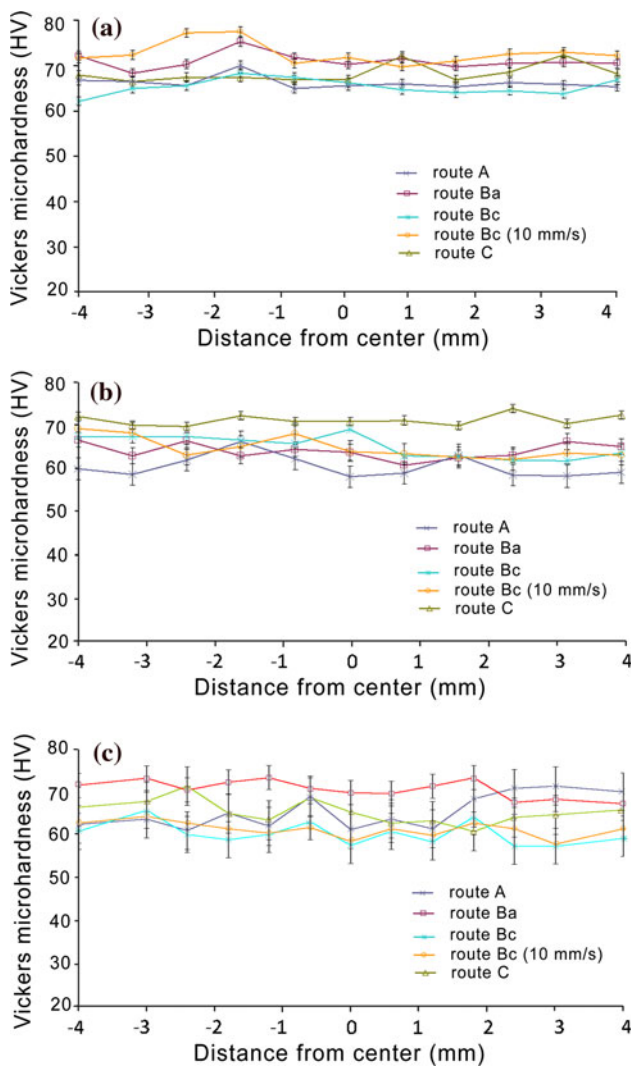
Fig. 6 Micro-hardness distribution over cross section of TCAP-processed samples after heat treatment. **a** in mode R1; **b** in mode R2; and **c** in mode R3

the annealing. The grain size is nearly uniform, especially after the higher extrusion rate (Fig. 7c). The sample deformed by the route *C* after this annealing mode (Fig. 7d) probably shows the highest heterogeneity of the grain sizes from all tested and investigated materials, although the refinement of the original bigger deformed grains also occurred in this sample.

R2 mode There is a slight growth of the grain size during route *A* after annealing (R2) in comparison with the R1 mode. Nevertheless, there are no visible signs of an abnormal grain growth in the microstructure (Fig. 8a). This phenomenon is sometimes called secondary recrystallization. It has been documented, for example, after ECAP and subsequent annealing of Cu [50]. Similar behavior is characteristic for route *Ba*. The microstructure of the sample extruded at the *Bc* route (5 mm/s) seems to be the

most stable from the standpoint of the grain coarsening (Fig. 8b). It can be seen (Fig. 8c) that different extrusion velocity caused different behavior of the microstructure. While in the case of lower velocity fine grains are distributed equally in the volume. At higher extrusion velocity very fine grains are visible in form of islands. The differences among the grain sizes increase after the strain on the route *C* and annealing in the R2 mode. A relatively large fraction of the small grains still remains intact.

XRD diffraction of Cu samples after TCAP and thermal processing

The evaluation of structural changes of the samples after annealing in R1–R3 was carried out on the samples extruded at the rate of 5 mm/s.

The annealing of the extruded samples causes processes on their structure that are demonstrated in Fig. 9a, b. The states after the deformation can be distinguished by means of the differences in the mosaic structure of the samples after the annealing. The states after the annealing accentuate the mosaic structure differences created by various ways of extrusion (A, Ba, Bc, and C) before annealing.

A, Ba routes (samples I, II) Thanks to the thermal processing in the modes R1–R3, the growth of all mosaic blocks took place in the samples I and II within the whole range of temperatures.

Bc route (sample III) The portion of "big" mosaic blocks >10 μm in size increases during the annealing in R1 (Fig. 9a). As can be seen, the portion increases even more with the growing temperature (R2) (Fig. 9b). The thermodynamic potential of the growing big mosaic blocks has increased as a consequence of the R3 mode. It was a consequence of accumulation of paracrystalline distortions (i.e., lattice distortions of the second kind) [51, 52]. It caused disintegration of the majority of the mosaic blocks. The energy created during the disintegration became a driving force of repeated growth of the mosaic blocks. This process can take place during the annealing in R3 mode. The repeated increasing of the portion of the big mosaic blocks in the structure was the final result of the annealing.

C route (sample IV) The sample IV already contained a higher amount of "big" mosaic blocks >10 μm in size before the thermal processing. The amount of mosaic blocks was higher in comparison with the sample III. These blocks coexisted with smaller mosaic blocks (<10 μm in size). The annealing R1 also caused an increase of the thermodynamic potential in a similar way as in the case of the C route. This potential has grown so much that it caused disintegration of nearly all blocks. The main reason

Fig. 7 Microstructure of processed copper and subsequently annealed in mode R1. **a** route *A* (5 mm/s); **b** route *Bc* (5 mm/s); **c** route *Bc* (10 mm/s); **d** route *C* (5 mm/s)
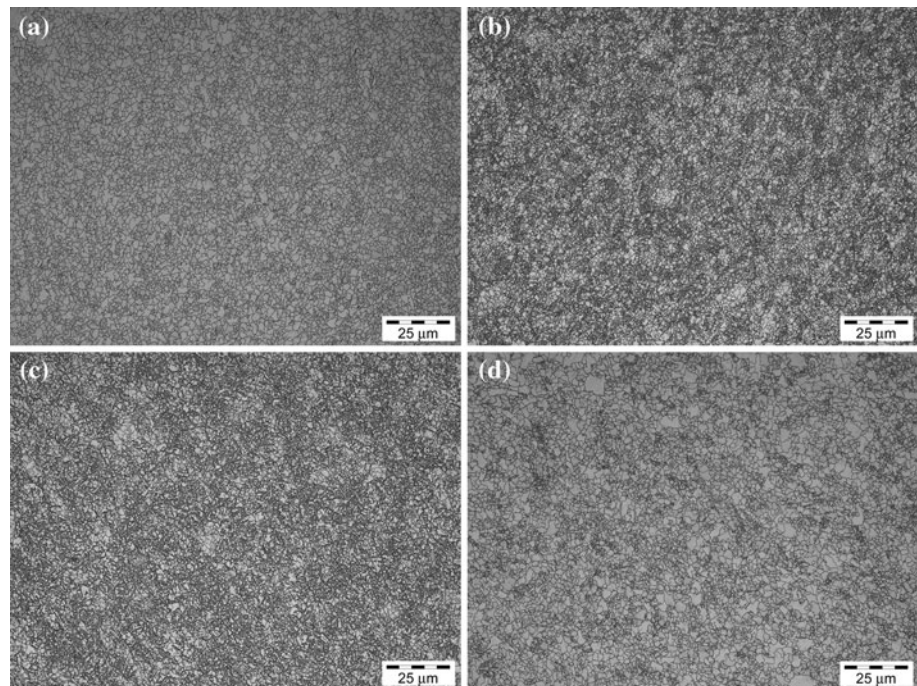
for the process in this case was also the accumulation of paracrystalline distortions that also increased interfacial energy of the structure. This worked later as a driving force of the repeated growth of the mosaic blocks during annealing in the modes R2 and R3.

The strain energy introduced by the extrusion to the samples I and II did not produce a subsequent (measurable) static recrystallization of the deformed samples at RT. Only the annealing initiated the recrystallization, which was higher, the higher the recrystallization temperature. The reversion process (disintegration of the mosaic structure) occurred in the sample I, especially in the case of applications of the modes R2 and R3.

The accumulated strain energy was higher in the samples III than in the samples I and II. It produced a subsequent static recrystallization of the deformed samples at RT. The recrystallization increased the size of the mosaic blocks even further during the annealing in the modes R1 and R2. The R3 mode caused an accumulation of the paracrystalline distortions in the mosaic blocks and their subsequent disintegration. As a result of this, there was an increase of the structure interfacial energy within blocks, which has become a driving force of the repeated growth of the mosaic blocks during annealing in the R3 mode (higher temperature).

The accumulated strain energy is even higher in the samples IV in comparison with the samples III, and it causes a subsequent static recrystallization of the deformed samples. The level of the recrystallization is higher than in the case of the sample III.

Finally, the recrystallized volume is also influenced in this way. It has caused an increase of the anchorage effect (pinning) of the boundaries of the new ("big") mosaic blocks in the prevailing non-recrystallized matrix. The effect is proportional to the quadrate of the size of the area occupied by the big blocks. It means that its influence has outweighed the decrease of Peierls–Nabarro stress in the volume occupied by the new big blocks. This stress is proportional to the cube of the size of the area occupied by the new big blocks.
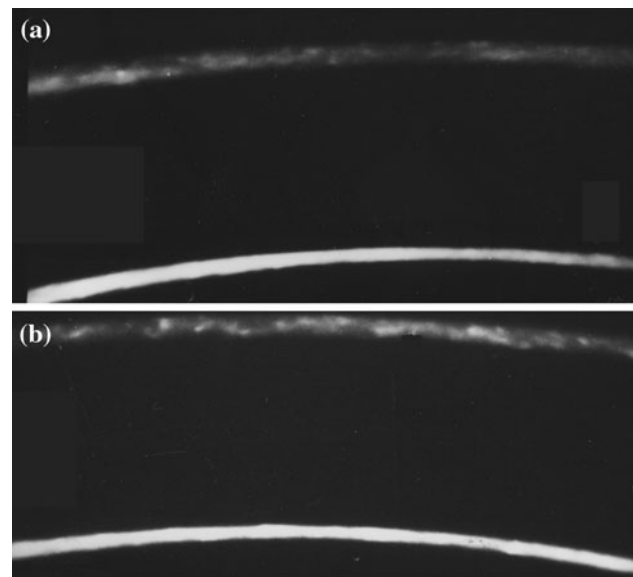
The recrystallization course continued by the annealing in the R1 mode. It produced further growth of the mosaic blocks. The accumulation of the paracrystalline distortions in the mosaic blocks took place again during this growth, which subsequently caused disintegration of these blocks; this means that the reversion process took place. The process again increased the interfacial energy of the structure. This energy has become a driving force of the repeated growth of the mosaic blocks. The higher the applied temperature, the further the recrystallization process in the modes R2 and R3 advanced.

As has been proved by Blum and Zeng [53], the deformed structures get rid of the strain-induced defects during the recrystallization. The "loss" of the imposed dislocations (or other defects) produces a considerable softening of the structure. Even "removal" of the severe strain effect can take place. The deformed grains can go through strain strengthening repeatedly during this process [54]. It is probable that the restoration decreases the driving force at higher strain rates. The driving force is necessary
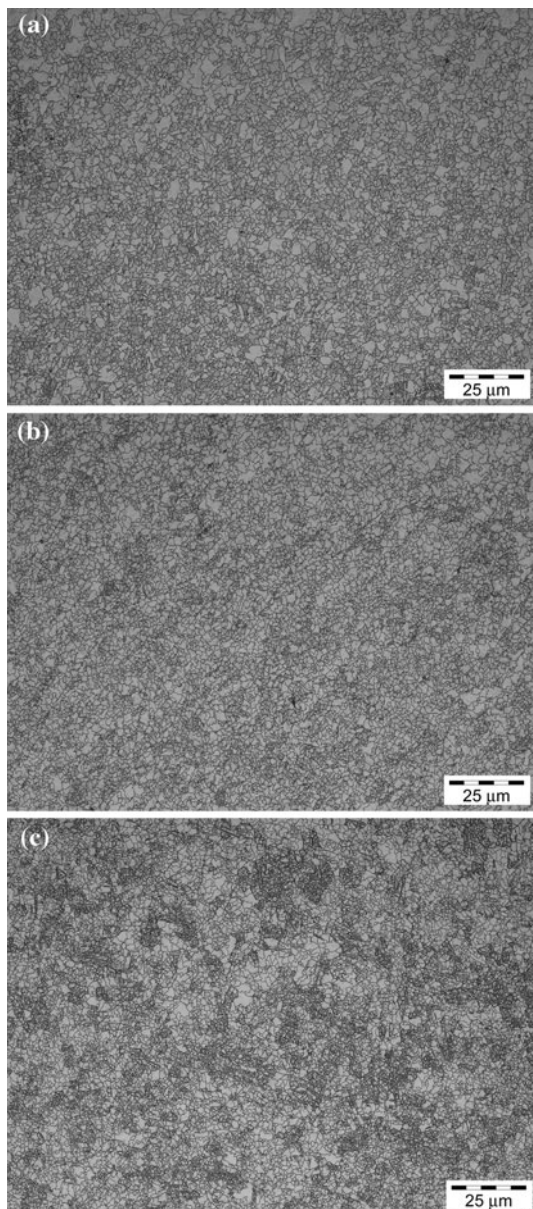
Fig. 8 Microstructure of processed copper and subsequently annealed in mode R2. **a** route *A* (5 mm/s); **b** route *Bc* (5 mm/s); and **c** route *Bc* (10 mm/s)

Fig. 9 X-ray diffraction lines of the planes (1 1 1) and (2 0 0). **a** route *Bc* (5 mm/s) and annealing in mode R1; and **b** route *Bc* (5 mm/s) and annealing in mode R2

They state that the nanocrystalline matrix may lose part of its strength after annealing even without significant grain growth.

Summary and conclusions

Cu (99.97%) was used as an experimental material in the TCAP process with the aim of determining an "optimum" strain path. The executed experiment has proved significant refinement of the microstructure in all used deformation paths. It has been shown that the processing path has a significant influence on the efficiency of TCAP processing in microstructural refinement as well as mechanical properties. In addition to this finding, the experiment has brought information on the course of the restoration processes. Analyzing the results we came to following conclusions:

(1) The *A* and *B* routes seem to be the most effective ways from the standpoint of the effectiveness of the grain refinement as well as achieved mechanical properties during the TCAP process. Relatively uniform distribution of micro-hardness through the sample cross section has been proved. It confirms the homogeneity of the imposed strain.

(2) The restoration processes came about in all samples extruded at the rate of 5 mm/s. The difference in the portion of restored structure is probably determined by the amount of accumulated energy during the

especially for the migration of boundaries and their mobility. If the value of the driving force is low, the material is stabilized against the recrystallization course. It means that the time necessary for the recrystallization is extended at higher temperatures. On the other hand, the strain can reduce the restoration effect at RT in the case of application of lower rates. The process of the recrystallization is accelerated afterwards. This can be used as an explanation of bimodal structures [55]. The conclusions and results obtained from the executed experiment are also supported by the results of Humphreys and Hatherly [56].

extrusion. The higher strain rate applied at the *Bc* route meant an exclusion of static recrystallization after the executed strain.

(3)　The higher value of ductility for the *C* route can be explained by the lower effectiveness of the strengthening (grain refinement) in comparison with other paths. The course of recrystallization after the strain at RT is the second possible explanation. The recrystallization of this sample took place in a bigger range than recrystallization of other samples.

(4)　The material extruded by the route *Bc* also went through the recrystallization at RT. Nevertheless, the range of the recrystallization was much smaller than in the case of the route *C*. The activation of different shear planes for the *Bc* route than for the route *C* may be the reason for this situation. It also means different effectiveness of the accumulation of the imposed strain.

(5)　The selected annealing modes have proved that the strain paths had different impacts on the thermal stability of processed samples. Except the route *C*, all specimens were quite stable up to 280 °C. Among others thermal treatment after TCAP brought almost uniform grain size, especially after the higher extrusion rate. If we consider the total number of passes, it is necessary to note that TCAP is very effective tool for grain refinement.

(6)　High effectiveness of the TCAP process is confirmed by the low number of passes in comparison with the classical ECAP process.

As it has been outlined, the TCAP process enables the application of mutations of existing known strain paths. Follow-up research should focus on these possibilities. Mapping of the sample rotation sense before extrusion should be the subject of further experiments.

References

1. Ma A, Jiang J, Saito N, Shigematsu I, Yuan Y, Yang D, Nishida Y (2009) Mater Sci Eng A 513–514:122
2. Munoz-Morris MA, Morfia DG (2010) Scr Mater 63:304
3. Wang Y, Chen M, Zhou F, Ma E (2002) Nature 419:912
4. Takata N, Lee SH, Tsuji N (2009) Mater Lett 63:1757
5. Vinogradov A, Patlan V, Suzuki Y, Kitagawa K, Kopylov VI (2002) Acta Mater 50:1639
6. Wei KX, Wei W, Wang F, Du QB, Alexandrov IV, Hu J (2011) Mater Sci Eng A 528:1478
7. Miyamoto H, Harada K, Mimaki T, Vinogradov A, Hashimoto S (2008) Corros Sci 50:1215
8. Valiev RZ, Krasilnikov NA, Tsenev NK (1991) Mater Sci Eng A 35:137
9. Valiev RZ, Langdon TG (2006) Prog Mater Sci 51:881
10. Segal VM (1995) Mater Sci Eng A 197:157
11. Valiev RZ, Estrin Y, Horita Z, Langdon TG, Zehetbauer MJ, Zhu YT (2006) JOM 58:33
12. Gertsman VY, Birringer R, Valiev RZ, Gleiter H (1994) Scr Metall Mater 30:229
13. Valiev RZ, Kozlov EV, Ivanov YF, Lian J, Nazarov AA, Baudelet B (1994) Acta Metall Mater 42:2467
14. Zhilyaev AP, Nurislamova GV, Kim BK, Baro MD, Szpunar JA, Langdon TG (2003) Acta Mater 51:753
15. Beygelzimer Y, Varyukhin V, Orlov D, Synkov S, Spuskanyuk A, Pashinska Y (2004) In: Zehetbauer MJ, Valiev RZ (eds) Nanomaterials by severe plastic deformation. Wiley-VCH Verlag, Weinheim
16. Varyutkhin VN, Beygelzimer Y, Synkov S, Orlov D (2006) Mater Sci Forum 335:503
17. Richert M, Liu Q, Hansen N (1999) Mater Sci Eng A 260:275
18. Chu HS, Liu KS, Yeh JW (2000) Metall Mater Trans A 31:2587
19. Wang QD, Chen YJ, Lin JB, Zhang LJ, Zhai CQ (2007) Mater Lett 61:4599
20. Toth LS, Lapovok R, Hasani A, Ch Gu (2009) Scr Mater 61:1121
21. Kocich R, Greger M, Kursa M, Szurman I, Macháčková A (2010) Mater Sci Eng A 527:6386
22. Gholinia A, Prangnell PB, Markushev MV (2000) Acta Mater 48:1115
23. Sun PL, Kao PW, Chang CP (2000) Mater Sci Eng A 283:82
24. Garcia-Infanta JM, Zhilyaev AP, Cepeda-Jimenez CM, Ruano OA, Carreno F (2008) Scr Mater 58:138
25. Nakashima K, Horita Z, Nemoto M, Langdon TG (2000) Mater Sci Eng A 281:82
26. Chakkingal U, Suriadi AB, Thomson PF (1999) Mater Sci Eng A 266:241
27. Toth LS, Beausir B, Guc CF, Estrin Y, Scheerbaum N, Davies CHJ (2010) Acta Mater 58:6706
28. Hoseini M, Meratian M, Toroghinejad MR, Szpunar J (2010) Mater Charact 61:1371
29. Furukawa M, Iwahashi Y, Horita Z, Nemoto M, Langdon TG (1998) Mater Sci Eng A 257:328
30. Iwahashi Y, Horita Z, Nemoto M, Langdon TG (1998) Acta Mater 46:3317
31. Iwahashi Y, Wang J, Horita Z, Nemoto M, Langdon TG (1996) Scr Mater 35:143
32. Oh-Ishi K, Horita Z, Furukawa M, Nemoto M, Langdon TG (1998) Metall Mater Trans A 29:2011
33. Segal VM (2002) Mater Sci Eng A 338:331
34. Embury JD, Poole WJ, Kohen E (1992) Scr Metall Mater 27:465
35. Zhu YT, Lowe TC (2000) Mater Sci Eng A 291:46
36. Li S (2009) Scr Mater 60:356
37. Liang W, Bian L, Xie G, Zhang W, Wang H, Wang S (2010) Mater Sci Eng A 527:5557
38. Srinivasan R (2001) Scr Mater 44:91
39. Suo T, Li Y, Guo Y, Liu Y (2006) Mater Sci Eng A 432:269
40. Mahallawy N, Shehata FA, Hameed M, Aal M, Kim HS (2010) Mater Sci Eng A 527:1404
41. Dobatkin SV, Szpunar JA, Zhilyaev AP, Cho JY, Kuznetsov AA (2007) Mater Sci Eng A 462:132
42. Beygelzimer Y, Varyukhin V, Synkov S, Orlov D (2009) Mater Sci Eng A 503:14
43. Kawasaki M, Figueiredo RB, Langdon TG (2011) Acta Mater 59:308
44. Akhmadeev NA, Kobelev NP, Mulyukov RR, Soifer YM, Valiev RZ (1993) Acta Metall Mater 41:1041

45. Lebedev AB, Burenkov YA, Romanov AE, Kopylov VI, Filonenko VP, Gryaznov VG (1995) Mater Sci Eng A 203:165
46. Zhang B, Shim VPW (2010) Acta Mater 58:6810
47. Del Valle JA, Perez-Prado MT, Ruano OA (2003) Mater Sci Eng A 355:68
48. Ion SE, Humphreys FJ, White SH (1982) Acta Metall 30:1909
49. Kadri SJ, Hartwig KT (2006) Mater Sci Forum 503–504:349
50. Molodova X, Gottstein G, Winning M, Hellmig RJ (2007) Mater Sci Eng A 460–461:204
51. Hindelah AM, Hosemann R (1988) J Phys C Solid State Phys 21:4155
52. Zei MS (1983) Phys Rev A 27:515
53. Blum W, Zeng XH (2009) Acta Mater 57:1966
54. Blum W, Li YJ, Durst K (2009) Acta Mater 57:5207
55. Hoppel HW, Zhou ZM, Mughrabi H, Valiev RZ (2002) Philos Mag A 9:1781
56. Humphreys FJ, Hatherly M (1996) Recrystallization and related annealing phenomena. Elsevier, Oxford